RESPONSE CHARACTERISTICS OF SATURATED CLAY TO IMPACT LOADING

Koichi AKAI* and Yukio YAMAUCHI**

SYNOPSIS

Earthquake can be considered to have two different characters, cyclic loading and random pulsative loading. As structures are apt to oscillate at their natural frequencies, the random pulsative loading is considered the important part of earthquake.

In the present study the dynamic response characters of soft saturated clays under an impact load have been investigated by subjecting the material to test under simply simulated earthquake in the triaxial cell. Three types of test adopted are those of the longitudinal impact vibration test, the torsional impact vibration test and the longitudinal forced vibration test.

INTRODUCTION

Since Japan lies on one of the notorious seismic bands in the world, we have suffered from much damage by a lot of intense earthquakes. There existed no reasonable aseismatic design for resisting terrible destructive earthquakes except the so-called seismic intensity method. As the technological development advances, most buildings extend their own heights more and more, and therefore, the conventional design is not applied to them. There came a new aseismatic design in which a structure is replaced by a discrete mass-spring-dashpot system, and responses to the seismic vibration are computed. The method is especially of great value for flexural buildings with multiple floor.

Comprehensive aseismatic design should take the behaviors of ground and the soil-structure interaction under seismic loading into account. This requirement has not been satisfied even partially because of the complexity in the mechanical properties of soils. In this paper a series of experimental results for saturated clays under various dynamic loadings is presented. The damping and dynamic stress-strain characteristics of clays are investigated in order to clarify the response characters of soft ground under earthquake.

* Prof. of Kyoto University, Yoshida Honmachi, Sakyo-ku, Kyoto
** Graduate course student, Kyoto University

LONGITUDINAL IMPACT VIBRATION TEST ON SATURATED CLAY

1. Soil Samples

Two kinds of soil, alluvial clay at Osaka and diluvial clay at Kyoto were tested. The former sample is termed No. 1 and the other No. 2. Their physical properties are tabulated in Table 1. These samples were mixed with water, care being taken to exclude fine air bubbles, then consolidated in a mould (25 cm in diameter, 15 cm in height), under the load of 0.2~1.0 kg/cm^2.

2. Testing Apparatus and Experimental Procedure

A block diagram of the longitudinal impact vibration apparatus is shown in Fig. 1. A specimen of clay, 3.5 cm in diameter and 8 cm high was fitted with a lucite cap and mounted on the pedestal of a triaxial cell. A rigid mass M was then lowered gently onto the cap of the specimen. At a given instant the string attaching the rigid mass to the counterweight was cut off, and the mass was released on the loading piston. The acceleration

Table 1. Physical properties of soil samples

Sample No.	No. 1	No. 2
Specific gravity	2.67	2.73
Clay fraction ($<5\mu$)	39%	23%
Silt fraction	44%	57%
Sand fraction	17%	20%
Moisture content*	40-50%	36-40%
Liquid limit	52.8%	48.9%
Plasticity index	27.2%	24.4%

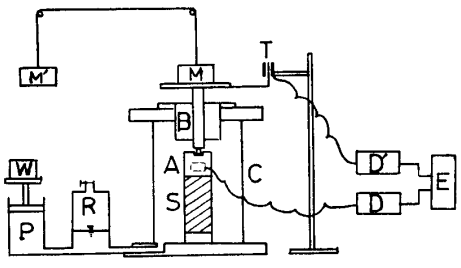

W : Weight
M : Weight
M' : Counterweight
C : Triaxial cell
S : Soil specimen
B : Ball bushing
A : Accelerometer
T : Transducer
D, D' : Amplifier
E : Electro-magnetic oscillograph
R : Air chamber
P : Constant-pressure cell

Fig. 1. Testing apparatus for the longitudinal impact vibration test

* Moisture contents of specimen tested are expressed in round number in the present paper, the variations being as high as ±0.5% in each case.

and displacement at the cap of the sample due to this sudden loading were recorded by an electric circuit. The accelerometer (allowable maximum capacity $\pm 2\,g$) was embedded in the lucite cap to ensure that it moved with the specimen. And a linear variable differential transducer was attached to the loading piston by a cantilever.

A ball bushing was attached to the triaxial cell so as to reduce the friction, if any, between the cell and loading piston. And an air chamber was connected to the triaxial cell, so that the loading piston moved easily regardless of confining water, and the variation of confining pressure resulted from the piston movement was minimized. A fresh specimen was used for every loading step and the weight was increased by every 0.4 kg until the specimen failed.

Another type of these impact vibration tests using a load cell was also conducted under unconfined condition in order to measure the applied load directly. In this case the load cell was set beneath the specimen as a pedestal.

3. Experimental Results

A typical record of acceleration, displacement and load is shown in Fig. 2. This figure indicates one of the records obtained by the test measuring the axial load under unconfined condition. It is seen that the records of displacement and load remarkably change at the first portion of vibration and that the load converges to a finite value, meanwhile the displacement shows an ordinary creep after the instantaneous portion. It can be also known from Fig. 2 that the first wave a_1 of acceleration record represents an apparent wave, for there would exist a corresponding stress wave if it

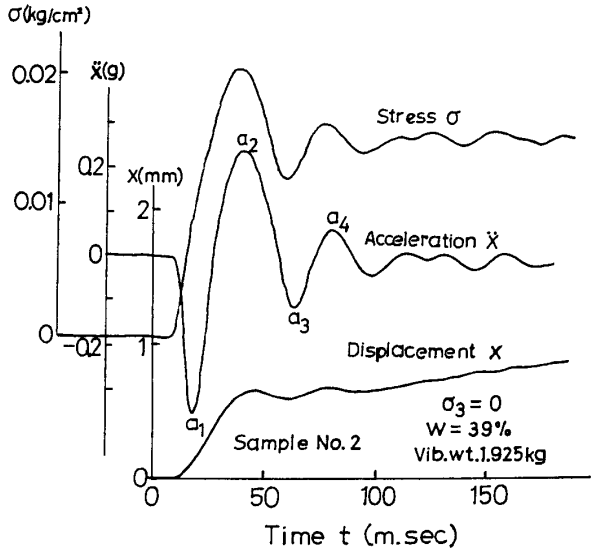

Fig. 2. Typical test record of the longitudinal impact vibration test

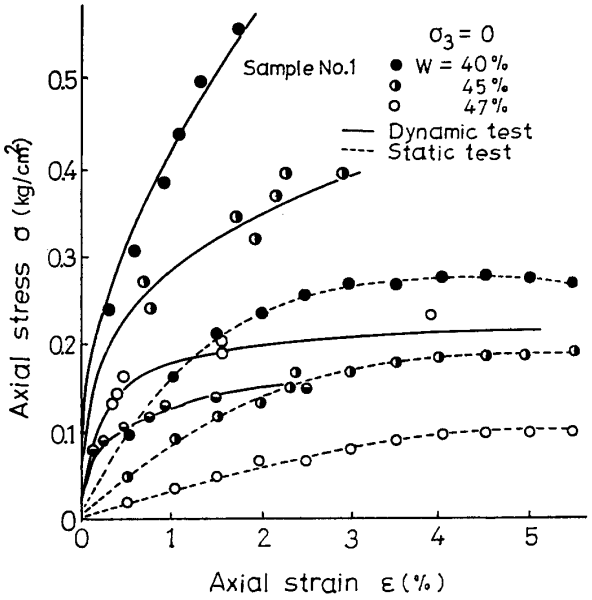

Fig. 3. Dynamic and static stress-strain relationships

were an actual wave. This part of acceleration wave results from the fact that the response frequency of the accelerometer did not fit for the measurement. Provided the response characteristics of the electric circuit which consists of an accelerometer, an amplifier and a recorder were excellent, the acceleration response corresponding to minus g would be recorded at time zero. The accelerometer used was a strain-gauge type which has high sensitivity, whereas the response frequency was somewhat low. Therefore, it has to be kept in mind that sometimes an apparent wave may be included in the record obtained.

(a) Dynamic stress-strain relationship

It has been recognized that the undrained shear strength of clay is closely related to the applied strain rate. Similar tendencies appear also in the present tests. The dynamic stress-strain relationships obtained by a series of tests with different loading weight are shown in Fig. 3.

In this test the vibration mass is calculated by the Rayleigh's method and, therefore, calculated from the rigid mass plus a contribution from the soil sample equal on one third the sample mass, considering the influence of sample mass on frequencies (Parmelee *et al.* 1964). Thus the dynamic stress is computed by

$$\sigma_d = \frac{1}{A_s} m(g + a_2) \qquad (1)$$

where σ_d is the dynamic stress, A_s the sectional area of a specimen, m a vibration mass, g the acceleration of gravity and a_2 the acceleration appeared

at the second wave in the record (See Fig. 2).

The corresponding average strain of the sample can be determined from the instantaneous elastic deformation in the observed record of sample displacement. The dotted lines in Fig. 3 represent the stress-strain relationships of samples by the static unconfined compression test. The rate of strain in the static test is equal to 1.25 %/min, whereas the average rate of strain calculated from the instantaneous displacement in the dynamic test is 500～2500 %/min, the latter being about 2000 times as fast as the former. Comparing the dynamic shear strength with the static one at the same axial strain under these conditions, it is seen that the dynamic shear strength is one and half or two times as large as the static one for every soil specimen with different water content as is seen in Fig. 3. The dynamic elastic modulus is also larger than the static one.

The dynamic stress-strain relationship in confined and unconfined tests are shown in Fig. 4. It can be seen from the figure that the dynamic shear strength is larger in the confined test than in the unconfined test. The

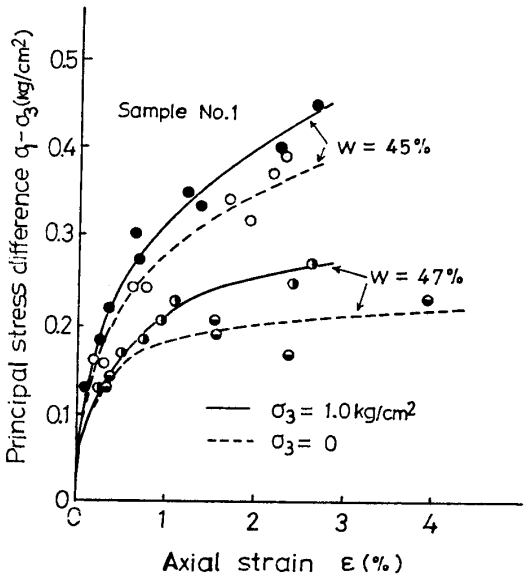

Fig. 4. Dynamic stress-strain relationships from confined and unconfined tests

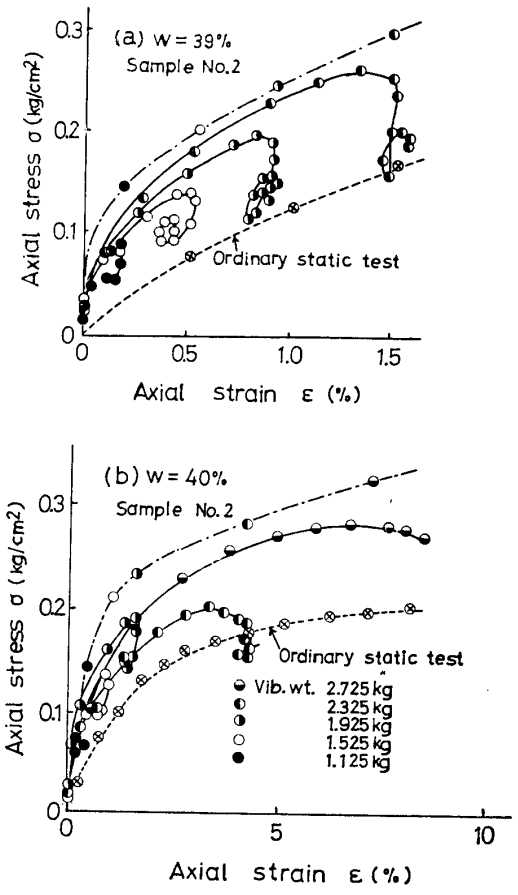

Fig. 5. Dynamic stress-strain relationships from a single test and a series of tests

variation in the confining pressure during the test was small, that is, only 20 to 30 g/cm^2.

In the impact test using a load cell, on the other hand, the dynamic stress at any time can be directly calculated from the observed load record and the corresponding average strains of the sample can be determined from the displacement record. By plotting the stress against the corresponding strain, dynamic stress-strain curves under these conditions are outlined as shown in Fig. 5. Fig. 5(a) shows the results for specimens with the moisture content of $w = 39\,\%$, while Fig. 5(b) indicates those for specimens of $w = 40\,\%$.

The upper curve in Figs. 5(a) and (b) represents the stress-strain relationship calculated by the dynamic stress using Eq. (1) and the instantaneous displacement, whereas the lower curve corresponds to that in the ordinary static unconfined test. The middle looped curves in these figures show the relationships obtained from the single impact test. The time interval from one point on these curves to the adjacent points on the same curve is constant and equal to 0.005 seconds. As the curves extend to the right, the loading weight changes by an increment of 0.4 kg.

The average rates of strain for the curves shown in Fig. 5 are 480 %/min, 1260 %/min, 1410 %/min and 1500%/min, respectively, in order of increase in loading weight. In other words the strain-rate effect of clay is clear in the figure. Looking at the loops, it will be noticed that the unloading portion of the loop tends to be vertical as the load increases. It can be understood that the vertical unloading portion indicates yielding of the sample because of no elastic recovery. Owing to the experimental error, these tendencies are not so remarkable in Fig. 5(b).

(b) Logarithmic decrement, spring constant and viscosity constant

Assuming that a soil specimen is represented by a Voigt model, the equation of motion is given by

$$m\ddot{x} + c\dot{x} + kx = 0 \qquad (2)$$

where m denotes the vibration mass, c the viscosity constant, k the spring constant, x the dynamic displacement and the dots represent differentiation with respect to time. Solving Eq. (2), we obtain

$$x = C_1 e^{-\frac{c}{2m}t} \cos\left\{\sqrt{\frac{k}{m} + \frac{c^2}{4m^2}}\, t + \theta\right\} \qquad (3)$$

where C_1 and θ are both integral constants and determined by the boundary conditions.

On the other hand the logarithmic decrement δ is represented by

$$\delta = \log_e \frac{x_n}{x_{n+1}} = \frac{1}{n} \log_e \frac{x_0}{x_n} = \frac{c}{2m} T = \frac{2\pi c}{\sqrt{4km - c^2}} \qquad (4)$$

where T is the vibration period. As the dynamic displacement, x, is given by Eq. (3) for the system, the logarithmic decrement can be calculated from the acceleration record of the sample. The logarithmic decrements calculated from the second and the third waves of the acceleration records, $2\log_e(a_2/a_3)$, increase with the vibration mass, whereas those calculated from the third, the fourth and the fifth, $2\log_e(a_3/a_4)$ and $2\log_e(a_4/a_5)$, are approximately constant, 1.0～2.0, regardless of the vibration mass.

The relationships between the moisture content of the clay specimen and the averaged logarithmic decrements are shown in Fig. 6. The dotted line in the figure represents the logarithmic decrement for the case of $\sigma_3 = 1.0$ kg/cm^2. It is seen clearly from the figure that the logarithmic decrement increases exponentially with increase in the moisture content of the sample. On the other hand, the logarithmic decrements obtained from the test with confining pressure are smaller than those from the test under unconfined condition. Therefore the vibration lasts longer and the clay sample behaves more elastically in the confined condition than that in the unconfined case. The black circle in Fig. 6 represents the logarithmic decrement obtained from the longitudinal forced vibration test described later.

Transforming Eq. (4), we obtain

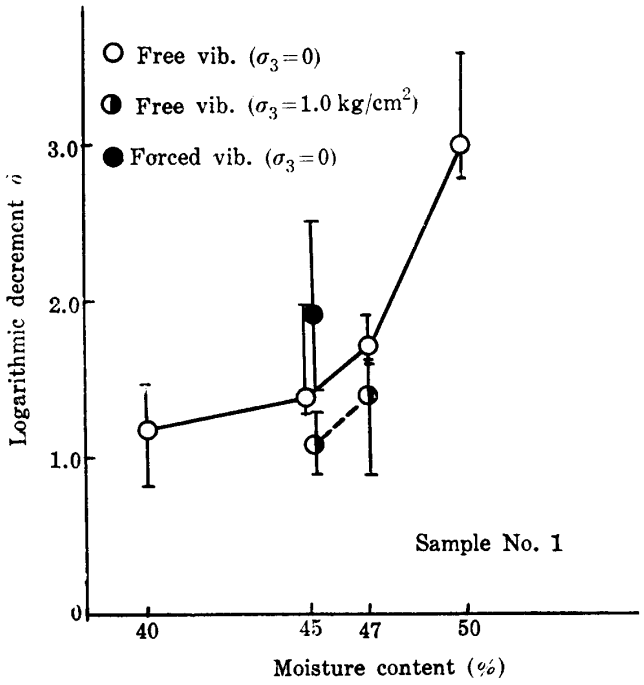

Fig. 6. Logarithmic decrement *vs.* moisture content

$$c = 2m\frac{\delta}{T} \tag{5}$$

$$k = \frac{m}{T^2}(\delta^2 + 4\pi^2) \tag{6}$$

The viscosity constant c and the spring constant k can be calculated from Eqs. (5) and (6), respectively, by substituting the logarithmic decrement δ and the period T into them. The correlations between the vibration mass and the viscosity constant and also the spring constant are shown in Figs. 7(a) and (b), respectively. The dotted lines in these figures denote the results obtained by the tests applying a confining pressure of $\sigma_3 = 1.0$ kg/cm^2 and the solid lines denote the results in unconfined conditions. It is seen from Fig. 7(a) that, for the same vibration mass, the viscosity constant becomes large and the sample seems to be more inelastic as the moisture content increases. It means that the vibration ceases more rapidly with increase in moisture content. When some confining pressure is applied, however, the viscosity constant decreases remarkably and the clay specimen,

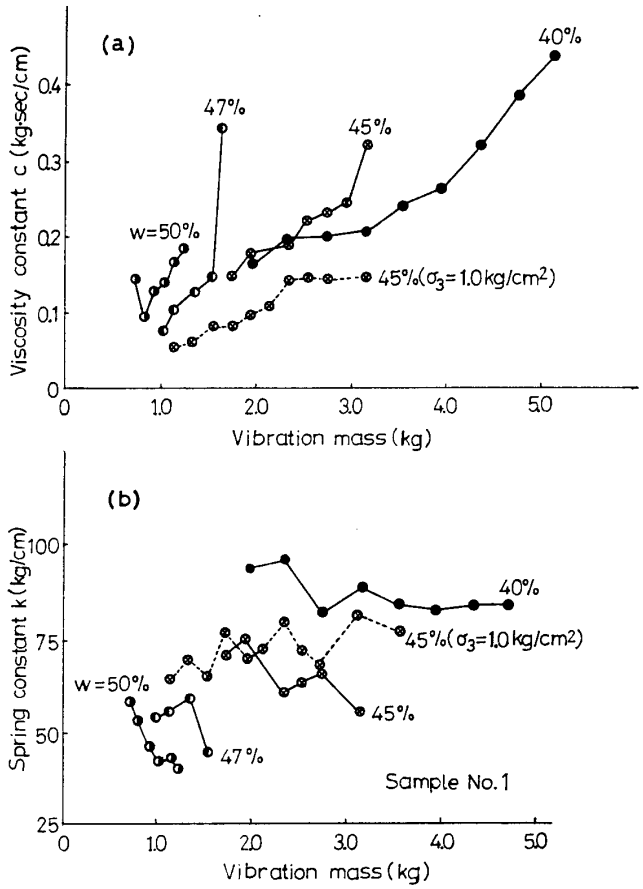

Fig. 7. Viscosity constant and spring constant *vs.* vibration mass

behaves more elastically. The linearity of response of the clay sample, represented by a Voigt model, disappears with increase in the vibration mass over the yielding value of the sample and, therefore, the adaptability of Eq. (5) also vanishes. On the other hand, it is recognized from Fig. 7(b) that the spring constant decreases with increase in the moisture content of the sample and it increases with the confining pressure.

Fig. 8 shows the average values of the viscosity constant and the spring constant corresponding to the moisture content of the sample. The dotted line in the figure shows the correlation between the spring constant and the moisture content and the viscosity constant *vs.* moisture content correlation is represented by the solid line. Both the spring constant and the viscosity constant decrease with increase in the moisture content of the sample. Because the moisture content of soil decreases with depth in normally consolidated ground, it is concluded that the spring constant increases with ground depth. In case of the viscosity constant, however, it is unreasonable to discuss about the damping of a ground, considering the accuracy of the test results.

The maximum values of the dynamic displacement are represented by

$$x = C_1 e^{-\frac{c}{2m}t} \qquad (7)$$

which means that they decrease exponentially with time. Thus the relationship between the maximum values of dynamic displacement and time is a straight line on a semi-logarithmic paper. The viscosity constant can be calculated from the gradient of this straight line. The above tendency is also

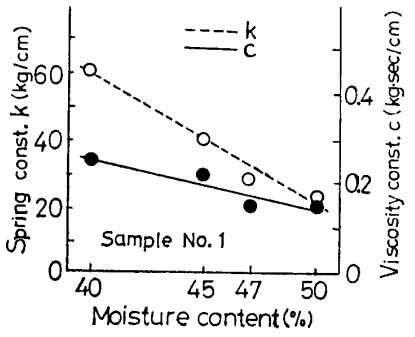

Fig. 8. Viscosity constant and spring constant *vs.* moisture content

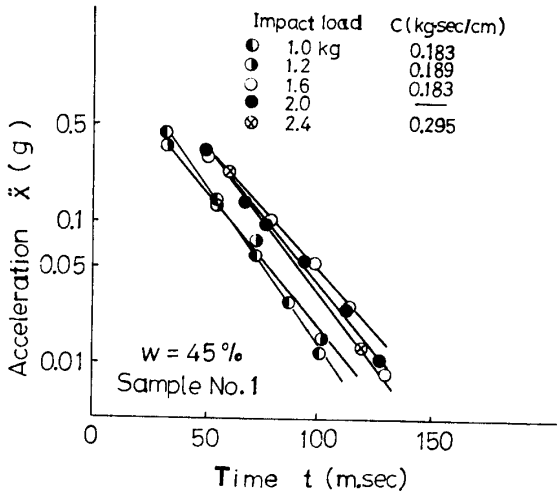

Fig. 9. Envelopes of the acceleration response wave

seen in the relationship between the acceleration and time (Akai *et al.* 1966). Fig. 9 shows relationships between the acceleration and time obtained from the records in which the moisture content of sample is about 45 %. It is seen from this figure that logarithm of the acceleration decreases approximately linearly with time. This means that the acceleration waves of the sample decrease exponentially; the clay specimen can be approximately represented by a Voigt model. In other words this figure implies that the clay has a linear elasticity and a linear damping characteristic. The viscosity constants calculated from the gradient of the straight lines in Fig. 9 are written in the figure and it will be recognized that these values are approximately equal to the corresponding values obtained by the method mentioned before.

The above analytical results show that the spring constant k and the viscosity constant c of clay structures can be calculated from the logarithmic decrement δ and the vibration period T in the free vibration test, based upon the theoretical equations (5) and (6). It should be noticed that, as an alternative method, they might be obtained by solving the differential equation of free vibration simultaneously. This method will be briefly discussed in the Appendix.

TORSIONAL IMPACT VIBRATION TEST ON SATURATED CLAY

1. Testing Apparatus and Experimental Procedure

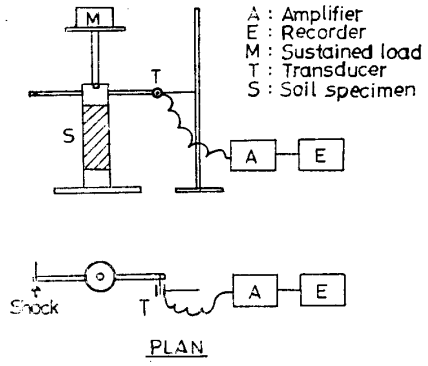

Fig. 10. Testing apparatus for the torsional impact vibration test

A block diagram of the torsional impact vibration apparatus is shown in Fig. 10. Electro-magnetic shocks were applied and the torsional displacements were measured by a linear variable differential transducer during the vibration generated by these shocks and they were recorded on an electro-magnetic oscillograph.

After the vertical creep under a given sustained load ceased, the shocks were generated by electro-magnet against the input voltage 50 V, 75 V and 100 V, and the displacements were measured. The tenth displacement after ten shocks was also recorded. Such tests were conducted for a series of sustained load. The interval between the electro-magnet and the iron piece was kept constant when the shocks were applied. The soil sample tested was the sample No. 2 described in the preceding section.

2. The Background Theory

A free torsional vibration of a bar occurs when a torque is applied

and removed suddenly. The angular position of the bar at a given time is determined by the angle from its position at rest. The spring constant k in this case is defined by the torque required to twist the sample by a unit angle. If we consider a round bar, h cm in length and d cm in diameter, we obtain

$$k = \frac{\pi d^4 G}{32h} \tag{8}$$

from the well-known equation concerning the torsional angle, where G is the shear modulus of the sample (Timoshenko *et al.* 1951).

The torque of the axis is equal to $k\theta$ when the axis is twisted by an angle θ during vibration. The differential equation of motion of a body rotating around the fixed axis is given by equating the moment of external force with the product of the angular acceleration and the moment of inertia around the axis. Thus we obtain

$$I\ddot{\theta} = -k\theta \tag{9}$$

where I denotes the moment of inertia around the axis for the rectangular bar and $\ddot{\theta}$ the angular acceleration. Using a symbol

$$p^2 = \frac{k}{I} \tag{10}$$

we obtain

$$\ddot{\theta} + p^2\theta = 0 \tag{11}$$

The solution of this equation is

$$\theta = \theta_0 \cos pt + \frac{\dot{\theta}_0}{p} \sin pt \tag{12}$$

where θ_0 and $\dot{\theta}_0$ denote the angular displacement and the angular velocity of the rectangular bar at time zero, respectively. From Eq. (12) the period T of the torsional vibration is given by

$$T = \frac{2\pi}{p} = 2\pi\sqrt{\frac{I}{k}} \tag{13}$$

Substituting Eq. (8), we obtain

$$G = \frac{128\pi h}{d^4 T^2} I \tag{14}$$

Considering the contribution of the mass of the sample by Rayleigh's

method (Goto 1957), we obtain

$$G = \frac{128\pi h}{d^4 T^2}\left(I + \frac{m}{6}d^2\right) \tag{15}$$

where m is the mass of the sample.

3. Experimental Results

One of the typical displacement records is shown in Fig. 11, where a small displacement occurs in the direction of the shock, and the amplitude of displacement decreases exponentially with time. The damping of the sample is not considered in Eq. (15). However Eq. (15) is considered to be valid for a clay sample even if the damping is ignored, because the damping does not influence the period so much.

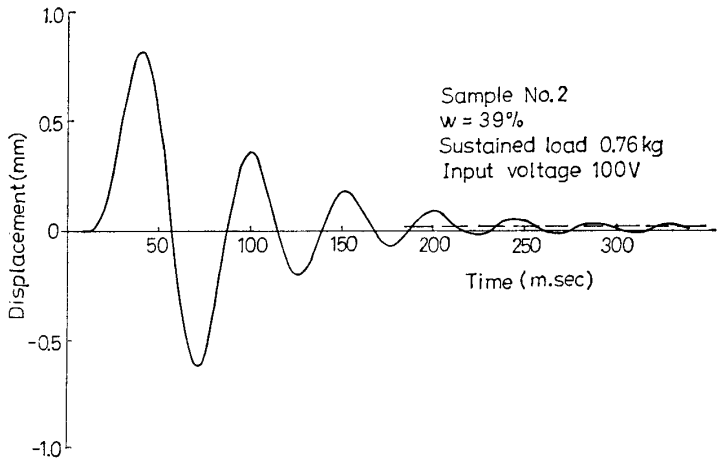

Fig. 11. Typical test record of the torsional impact vibration test

(a) Shear modulus of elasticity

Relationship between the vibration period and the sustained load are shown in Fig. 12(a) and the input voltage of the electro-magnetic shock *vs.* period relationships are in Fig. 12(b). It is seen from these figures that the vibration period of the sample is approximately constant with respect not only to the sustained load but to the input voltage, and the period for the sample with high moisture content is larger than that for low moisture content. As the shear modulus of elasticity varies inversely to the period, the shear modulus for the sample with high moisture content is smaller than for the hard sample. The results for the tenth shock are also shown in Fig. 12(b), where there exists little influence by repetition. This may result from the fact that the shocks were small.

In principle the correlation between the shear modulus of elasticity G and the Young's modulus E is represented by

$$G = \frac{E}{2(1+\mu)} \tag{16}$$

where μ is the Poisson's ratio. The Young's modulus of the clay sample with the moisture content of 39 % is approximately equal to 57 kg/cm^2 in the longitudinal impact vibration test and, therefore, the shear modulus of elasticity obtained from the torsional impact vibration test is fairly large as shown in Fig. 12(a), for $E = 3G$ when $\mu = 0.5$. This would be due to the fact that the influence of the viscosity of the sample is negleceted here. It is noted that, for each group of sample with different moisture contents, the shear modulus of elasticity is approximately constant regardless of the sustained load; that is, the elastic behaviors of clay under a transverse loading maintain its virginity even though it has been subjected to a vertical loading as high as the yielding load of the sample. The reason may be due to the saturation of the sample. This phenomenon is considered to take place only in saturated clays, however, it will be interesting as main shocks of an earthquake consist of distortional waves.

(b) Logarithmic decrement

As described previously the origin of a displacement record shifted in the

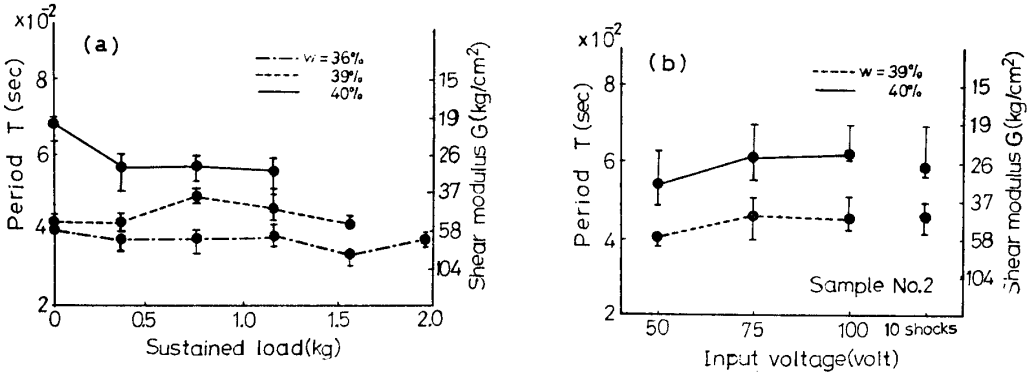

Fig. 12. Relationships between the vibration period, the shear modulus of elasticity, the sustained load and the input voltage

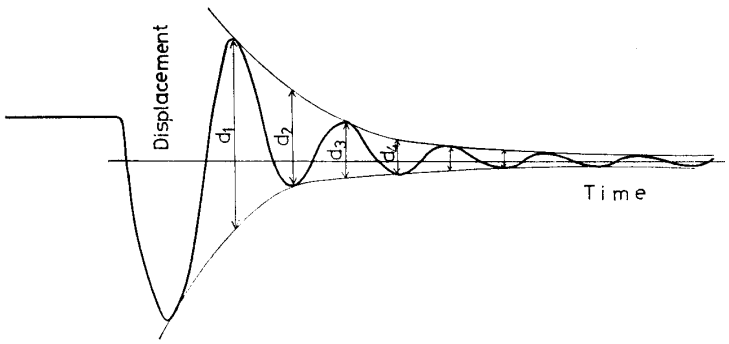

Fig. 13. Method of obtaining the displacement amplitude

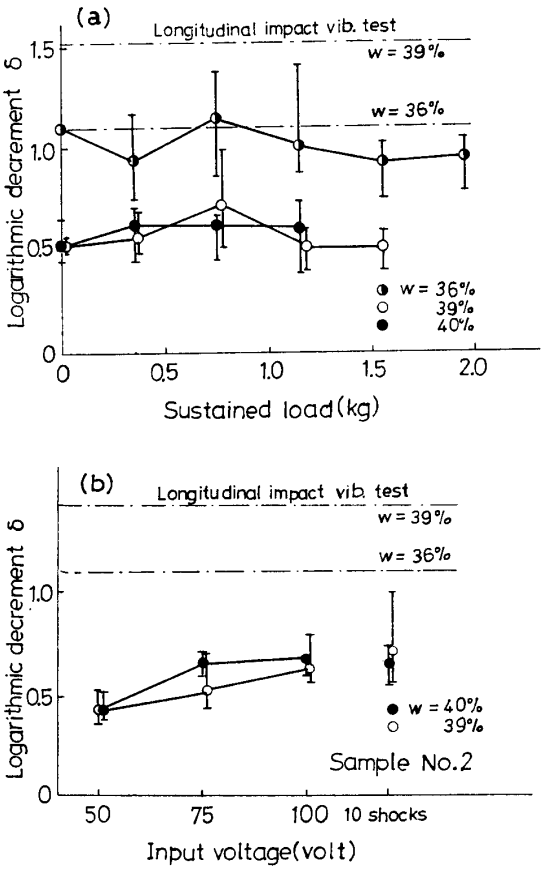

Fig. 14. Relationships between the logarithmic decrement, the sustained load and the input voltage

direction of the shock during the vibration and, therefore, the logarithmic decrement was calculated as follows: **i.** draw envelopes of the displacement records; **ii.** assume the vertical distance d_1, d_2, etc. between two envelopes at the maximum values of the displacement record as the full amplitude, as shown in Fig. 13.

The logarithmic decrement *vs.* the sustained load relationships are illustrated in Figs. 14(a) and (b). The logarithmic decrements δ in these figures are the averaged values computed from the displacement waves, from d_2 through d_7. And the upper straight lines represent the averaged values from the longitudinal impact vibration test. It is seen from Fig. 14(a) that the logarithmic decrement is approximately constant regardless of the sustained load. Therefore it is concluded that the damping characteristics of the sample are not influenced by the sustained load. As is clear in this figure the logarithmic decrement calculated from the longitudinal impact vibration test is about twice as large as that calculated from the torsional impact vibration test. On the other hand, there exists a tendency that the logarithmic decrement increases with the input voltage as shown in Fig. 14(b).

LONGITUDINAL FORCED VIBRATION TEST ON SATURATED CLAY

1. Testing Apparatus and Experimental Procedure

A block diagram of the longitudinal forced vibration apparatus is shown in Fig. 15. The vertical vibration generated by a cam is transformed (by a bellows into the vibration of water pressure) and the vibration in pressure is changed by another bellows into vertical vibration again, and then sinusoidal load is applied to the soil specimen through the load cell and the loading piston. The bellows for axial stress and the bellows guide are fixed to the same frame, and the diaphram type pressure gauge (allowable capacity 5 kg/cm^2) for measuring the axial stress is fixed to the bottom of the bellows. The rotation of a motor is transmitted to the cam axis through two gear systems that can regulate the frequency of the rotation up to an arbitrary value without gear change. The axial stress is kept constant by expanding the bellows by a stressing piston. To minimize the vibration in confining pressure a long vinyl pipe is used.

The load generated in this way was applied to the soil specimen till the

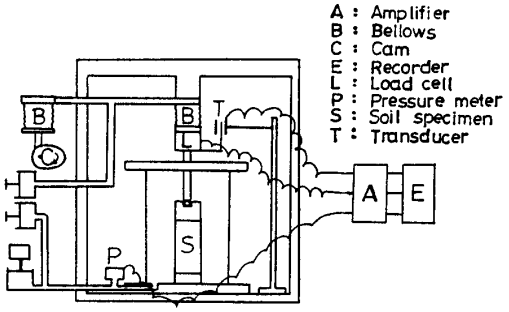

Fig. 15. Testing apparatus for the longitudinal forced vibration test

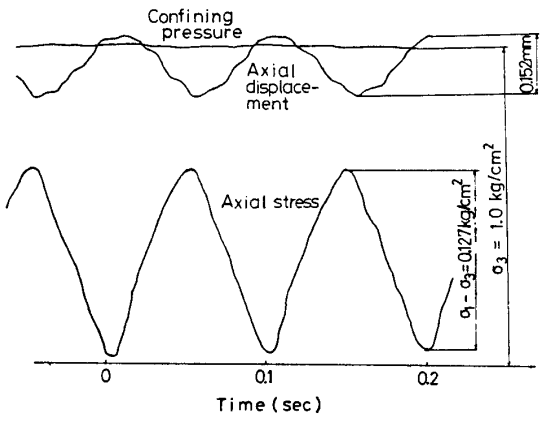

Fig. 16. Typical test record of the longitudinal forced vibration test

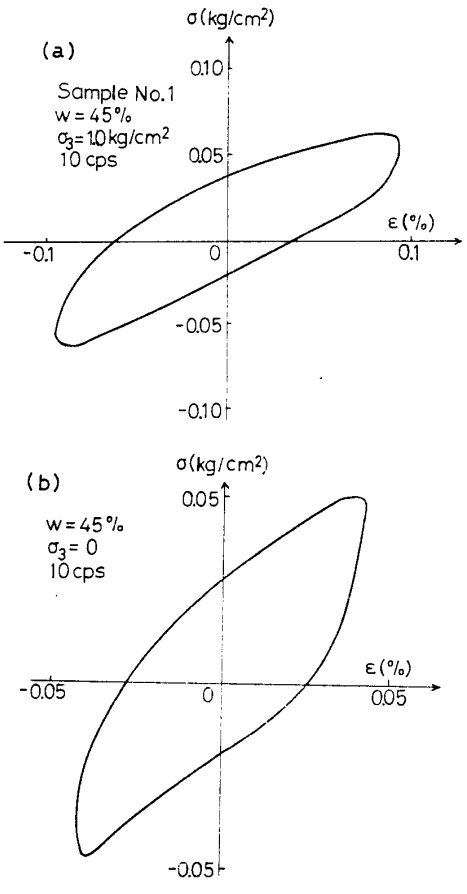

Fig. 17. Stress-strain relationship under cyclic loading

steady state occurred and, then, the axial vibration displacement and the axial vibration stress were measured by the linear variable transducer and the load cell, respectively, and recorded on an electro-magnetic oscillograph. The variation in confining pressure during the test was little. The sample No. 1 was used for this test.

2. Experimental Results

A typical record of the displacement and the stress is shown in Fig. 16. Changes in the axial stress, axial displacement and confining pressure are shown in the figure. These records are not perfectly sinusoidal because of the existence of noise and distortion.

The stress-strain relationships calculated from the above records are shown in Fig. 17. Fig. 17(a) indicates the stress-strain relationship for the sample of $w = 40$ % under the frequency of axial stress is 10 cps and the confining pressure of 1 kg/cm^2. On the other hand, Fig. 17(b) shows the stress-strain relationship in the unconfined condition.

Let us define the ratio of the axial stress amplitude to the axial strain amplitude as an apparent modulus of elasticity. On the other hand, the logarithmic decrement can be approximately calculated from the damping energy. The specific damping ψ is defined as the ratio of the dissipated energy D to the maximum potential energy W_0 during the same cycle in the forced vibration (Freudenthal 1954). ψ is also defined as the decrement of the vibration energy for one cycle in the free vibration. Therefore we obtain

$$\psi = \frac{D}{\Delta N}\frac{1}{W_0} = \frac{d \log W_0}{\Delta N} \tag{17}$$

where N is the total number of the loading cycle and $\Delta N = 1$. Provided that the energy varies proportionally to the square of the stress amplitude, we obtain the correlation

$$\psi = 2\delta \tag{18}$$

When the cyclic force $p = p_0 \sin \omega t$ is applied and the resultant maximum deformation velocity is v_0, the rate of energy loss is

$$\dot{D} = \frac{1}{2} p_0 v_0 \sin \theta \tag{19}$$

where θ is the angle by which the cyclic strain vector lags behind the cyclic stress vector during sinusoidal loading to a visco-elastic material. The relationship between the velocity v_0 and the displacement amplitude A_0 is represented by

$$v_0 = \omega A_0 = 2\pi n A_0 \tag{20}$$

where n denotes a positive integer equal to the number of loading cycle. Therefore Eq. (19) becomes

$$\dot{D} = \frac{1}{2}\omega p_0 A_0 \sin\theta \fallingdotseq \frac{1}{2}\omega p_0 A_0 \theta = n\pi p_0 \theta \tag{21}$$

when θ is small. The dissipated energy per cycle and the maximum storage energy per cycle are represented respectively by

$$D = \pi p_0 A_0 \theta \tag{22}$$

$$W_0 = \frac{1}{2} p_0 A_0 \tag{23}$$

Thus we obtain from Eqs. (17), (18), (22) and (23),

$$\delta = \frac{\psi}{2} = \pi\theta = \frac{D}{p_0 A_0} \tag{24}$$

where p_0 refers to the full amplitude of axial stress, A_0 the amplitude of axial strain and D the dissipated energy, *i.e.*, the area of the ellipse in Fig. 17.

The logarithmic decrement δ and the apparent Young's modulus E are tabulated in Table 2. The value of E in this table is a little larger than that calculated from the longitudinal impact vibration test. It may be considered that this difference results from the difference in definition of the modulus. Actually the reverse case may occur by reason of sample disturbance. On the other hand, the value of the logarithmic decrement, $\delta = 1.5 \sim 2.5$, is also a little larger than that from the impact vibration test, where $\delta = 1.0 \sim 2.0$ as shown in Fig. 6. This may result from the fact that the clay sample was disturbed due to application of cyclic load.

In Fig. 18 is indicated the correlation between logarithm of the maximum

Table 2. The Young's modulus E and the logarithmic decrement δ from the longitudinal forced vibration test for $w \fallingdotseq 45$ % samples

Confining pressure (kg/cm²)	Frequency (cps)	Stress amplitude (kg/cm²)	Young's modulus E (kg/cm²)	Logarithmic decrement δ
1.0	10	0.127	84	1.45
1.0	10	0.214	129	2.49
1.0	10	0.204	119	1.62
0	10	0.110	152	1.59
0	10	0.147	113	1.90
0	5	0.118	171	1.51

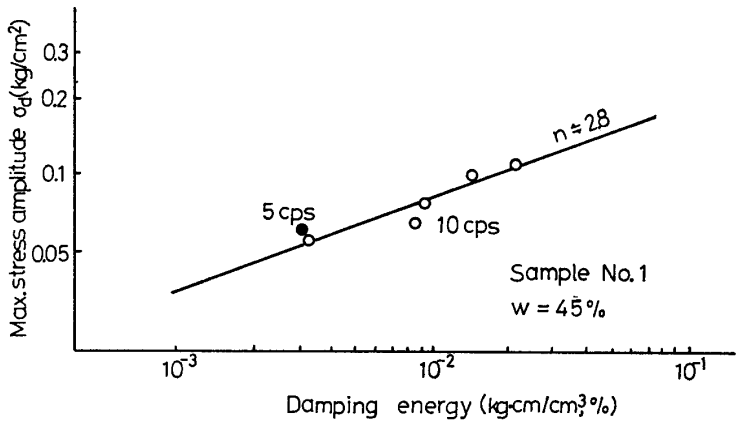

Fig. 18. Damping energy *vs.* maximum stress amplitude

stress amplitude and logarithm of the damping energy D. The open circles and the black circle in the figure correspond to the test under 10 cps and 5 cps, respectively. Drawing a straight line passing through these plots, we can compute the values of n from its gradient:

$$n = \frac{\Delta \log D}{\Delta \log \sigma_d} \fallingdotseq 2.8 \tag{25}$$

As the sample used in the longitudinal forced vibration test (sample No. 1) is different from that used in the torsional impact vibration test (sample No. 2), the value of n cannot directly be compared with each other. Taylor and Hughes have reported that the n value of clay is in the range of 1.82 to 2.15 (Taylor *et al.* 1965). Thus the present result ($n \fallingdotseq 2.8$) is considered to show the dependency of the damping characteristics of clay on the stress amplitude. The fact that the value of n is equal to about 2.8, however, means that the damping of clay would be nearly the viscous damping.

As already mentioned the value of the logarithmic decrement δ is approximately constant irrespective of the sustained load. It means the damping characteristics of clay sample are not influenced by the sustained load. It has been also concluded in the preceding section that the shear modulus of elasticity is not influenced by the sustained load. Considering these results, it will be noted that the response of clay ground to the main shocks of an earthquake is not influenced by the sustained load, with the exception of inertia force. This would be one of the most important aspects to be considered when one engages himself with the aseismatic design of structures on or under the clay ground.

CONCLUSIONS

Throughout the experimental investigations described in the present paper some interesting and important conclusions can be summarized as follows.

(1) The undrained shear strength of saturated clay obtained from the dynamic test is one and half or two times that from the static test, and it increases with the confining pressure.

(2) The stress-strain relationship calculated by a series of vibration mass (by means of Rayleigh's method), acceleration records and axial strains at instantaneous displacement coincides approximately with that computed from the loading and displacement records of single test.

(3) The logarithmic decrement δ for saturated clay increases with the moisture content, and the damping tends to decrease with the confining pressure.

(4) The value of the spring constant k computed from the logarithmic decrement δ and the vibration period T, by assuming that the soil sample can be represented by a Voigt model, is approximately constant with vibration mass, while it decreases with increase in the moisture content of the specimen. If the vibration mass is constant, the viscosity constant c increases with the moisture content, however, the absolute value decreases linearly with moisture content. Both the spring constant k and the viscosity constant c seem to be dependent on the confining pressure.

(5) Logarithm of the maximum values in the acceleration record in the longitudinal impact vibration test is approximately linear with time. Then it is able to get the viscosity constant c from the gradient of this straight line.

(6) The shear modulus of elasticity G and the logarithmic decrement δ obtained from the torsional impact vibration test are not influenced by the sustained load.

(7) The logarithmic decrement δ obtained by the longitudinal impact vibration test greatly differs from that obtained by the torsional impact vibration test. This means that the damping of clay is dependent on the stress amplitude. The damping of clay depends upon the stress amplitude acting in the direction of vibration, whereas it is independent of the stress perpendicular to it.

(8) The correlation between the damping energy and the corresponding stress amplitude in the forced vibration test becomes linear on logarithmic plotting. The gradient of the line n shows the degree of dependence on stress amplitude. The value $n \fallingdotseq 2.8$ was obtained in the present test.

(9) Considering the conclusions (4)-(8) synthetically, it may be considered that the saturated clay is approximately represented by a Voigt model, however, elements of which (spring and dashpot) are non-linear to some extent.

REFERENCES

Akai, K., Y. Yamauchi and M. Tokuda, 1966. Response characteristics of saturated clay to impact loading (in Japanese). Proc. Japan Earthquake Eng. Symp., Tokyo, pp. 91-96.

Freudenthal, A. M., 1954. Structural engineering aspect, Building materials—their elasticity and inelasticity. edited by M. Reiner, North-Holland, Amsterdam, pp. 80-86.

Goto, S., 1957. Dynamical properties of compacted soils. Rep. on Researches and Investigations 1955-1956, Japan Society of SMFE, pp. 22-24.

Parmelee, R. A., J. Penzien, C. F. Scheffey, H. B. Seed and G. R. Thiers, 1964. Seismic effect on structures supported on piles extending through deep sensitive clays. Rep. to Calif. State Division of Highways, No. 14247.

Taylor, P. W. and J. M. O. Hughes, 1965. Dynamic properties of foundation subsoils as determined from laboratory tests. Proc. 3rd World Conf. on Earthquake Eng., 2, Auckland & Wellington, pp. 1-14.

Timoshenko, S. P. and J. N. Goodier, 1951. Theory of elasticity. McGraw-Hill, New York, pp. 258-264.

APPENDIX

Spring Constant k and Viscosity Constant c Computed by Simultaneous Equations.

The equation of motion for a single-degree-of-freedom system is represented by Eq. (2):

$$m\ddot{x}+c\dot{x}+kx = 0 \tag{A-1}$$

where m is the vibration mass, c the viscosity constant, k the spring constant and x the dynamic displacement.

When the direction of vibration coincides with that of the gravity, a Voigt model supporting mass m shows a displacement statically

$$x_s = mg/k \tag{A-2}$$

where x_s is called sag. To distinguish dynamic displacement from the static sag x_s, let it be termed x_d. Choosing the lower end of a Voigt model with no load as the origin for displacement, the equation of motion is represented as

$$m\frac{d^2}{dt^2}(x_s+x_d) + c\frac{d}{dt}(x_s+x_d)+k(x_s+x_d) = mg \tag{A-3}$$

As $\ddot{x}_s = \ddot{x}_d = 0$ and $kx_s = mg$ in Eq. (A-3) we can write Eq. (A-3) as

$$m\ddot{x}_d+c\dot{x}_d+kx_d = 0 \tag{A-4}$$

Therefore Eq. (A-4) coincides with Eq. (A-1). Postulating that the values of the spring constant and the viscosity constant do not vary and that the values of acceleration, velocity and dynamic displacement are known at a

given time, we obtain next simultaneous equations by substituting them into Eq. (A-1).

$$\left.\begin{aligned} m\ddot{x}_1+c\dot{x}_1+kx_1 &= 0 \\ m\ddot{x}_2+c\dot{x}_2+kx_2 &= 0 \end{aligned}\right\} \qquad \text{(A-5)}$$

where $\ddot{x}_1$, $\dot{x}_1$ and x_1 represent the acceleration, velocity and dynamic dis-

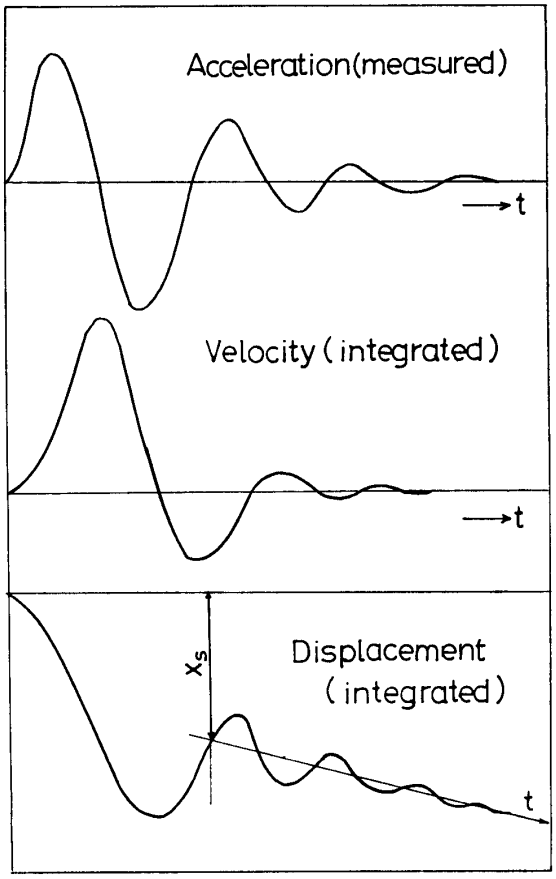

Fig. A-1. Velocity and displacement by integration of acceleration record

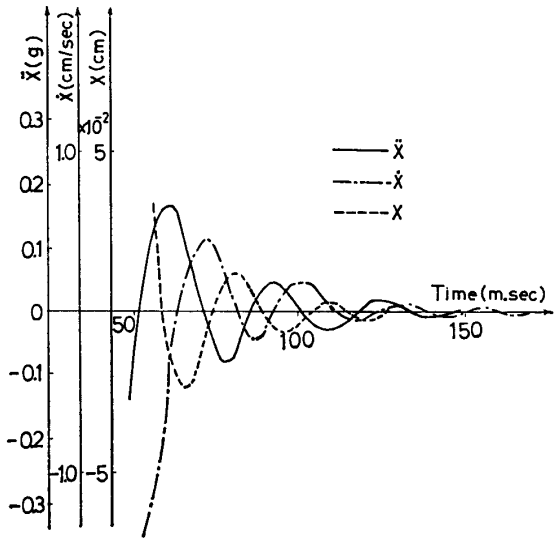

Fig. A-2. Acceleration, velocity and displacement in free vibration

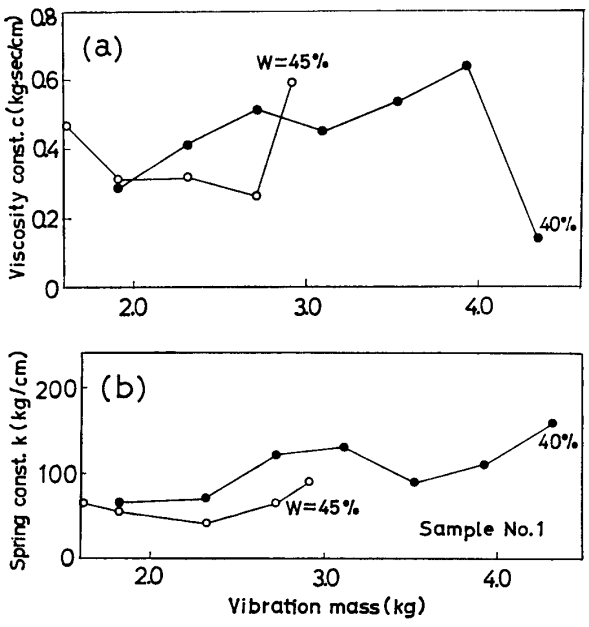

Fig. A-3. Viscosity constant and spring constant *vs.* vibration mass

placement at time t_1, respectively, and $\ddot{x}_2$, $\dot{x}_2$ and x_2 are those at t_2.

Displacements and velocities in Eq. (A-5) can be calculated by integrating the acceleration records. Because the acceleration records contain the false wave a_1 as mentioned in the present paper, the displacement-time diagram is computed by integrating the velocity-time diagram backward with respect to time, starting from a point where the vibration has ended. The displacment thus computed contains sag so that the dynamic displacement has to be determined by the method indicated in Fig. A-1: the centre of vibration is determined and a straight line is drawn as shown in the figure, considering the creep. This line corresponds to the abscissa for dynamic displacement.

The acceleration, velocity and displacement obtained by the above-mentioned method are shown in Fig. A-2. From this figure the spring constant and the viscosity constant at a given time can be calculated.

Values of the viscosity constant and the spring constant obtained by the above method are plotted against the vibration mass in Figs. A-3(a) and (b), respectively. A considerable scatter of the results in the figures may be due to the approximate integration and uncertainties in calculating the dynamic displacement.